# Diet Induced Obesity and Diabetes Enhance Mortality and Reduces Vaccine Efficacy for SARS-CoV-2

Robert M Johnson[1], Jeremy Ardanuy[1], Holly Hammond[1], James Logue[1], Lian Jackson[1], Lauren Baracco[1], Marisa McGrath[1], Carly Dillen[1], Nita Patel[2], Gale Smith[2], Matthew Frieman[1]

1. Center for Pathogen Research, Department of Microbiology and Immunology, University of Maryland School of Medicine, Baltimore, MD, 20201
2. Novavax, Gaithersburg, MD.

**Abstract**

Severe Acute Respiratory Syndrome Coronavirus-2 (SARS-CoV-2), the causative agent of Coronavirus disease 2019 (COVID-19), emerged in Wuhan, China, in December 2019. As of October 2022, there have been over 625 million confirmed cases of COVID-19, including over 6.5 million deaths. Epidemiological studies have indicated that comorbidities of obesity and diabetes mellitus are associated with increased morbidity and mortality following SARS-CoV-2 infection. We determined how the comorbidities of obesity and diabetes affect morbidity and mortality following SARS-CoV-2 infection in unvaccinated and adjuvanted spike nanoparticle (NVX-CoV2373) vaccinated mice. We find that obese/diabetic mice infected with SARS-CoV-2 have increased morbidity and mortality compared to age matched normal mice. Mice fed a high-fat diet (HFD) then vaccinated with NVX-CoV2373 produce equivalent neutralizing antibody titers to those fed a normal diet (ND). However, the HFD mice have reduced viral clearance early in infection. Analysis of the inflammatory immune response in HFD mice demonstrates a recruitment of neutrophils that was correlated with increased mortality and reduced clearance of the virus. Depletion of neutrophils in diabetic/obese vaccinated mice reduced disease severity and protected mice from lethality. This model recapitulates the increased disease severity associated with obesity and diabetes in humans with COVID-19 and is an important comorbidity to study with increasing obesity and diabetes across the world.

Corresponding author:
Matthew Frieman, PhD., Department of Microbiology and Immunology, University of Maryland School of Medicine, Baltimore, MD. mfrieman@som.umaryland.edu

33 **Importance**

34

35 SARS-CoV-2 has caused a wide spectrum of disease in the human population, from
36 asymptomatic infections to death. It is important to study the host differences that may alter the
37 pathogenesis of this virus. One clinical finding in COVID19 patients, is that people with obesity or
38 diabetes are at increased risk of severe illness from SARS-CoV-2 infection. We used a high fat diet model
39 in mice to study the effects of obesity and Type 2 diabetes on SARS-CoV-2 infection as well as how these
40 comorbidities alter the response to vaccination. We find that diabetic/obese mice have increased
41 disease after SARS-CoV-2 infection and they have slower clearance of virus. We find that the lungs of
42 these mice have increased neutrophils and that removing these neutrophils protect diabetic/obese mice
43 from disease. This demonstrates why these diseases have increased risk of severe disease and suggests
44 specific interventions upon infection.

45

46 **Introduction**

47 The United States of America has an obesity rate of 42%, diabetes rate of 11%, and 35 % of the
48 population has been identified as prediabetic[1]. Diabetes and obesity have been linked both clinically
49 and through physiological studies to increased severity of many types of diseases that can be traced
50 toward various aspects of these metabolic syndromes[2-4]. Epidemiologic studies of COVID-19 have
51 identified obesity and diabetes as significant risk factors for increased disease severity, length of
52 hospitalization, and death[5-10]. The immune and molecular mechanisms behind this increased risk of
53 COVID-19 have yet to be fully determined. SARS-CoV-2 is not the only coronavirus that displayed
54 increased disease severity in those with diabetes or obesity [6, 11-17]. The Middle East respiratory
55 syndrome coronavirus (MERS-CoV), first identified in 2012, was clinically and experimentally linked to
56 increased disease severity in those with diabetes[18, 19]. Across multiple clinical and epidemiological
57 studies, diabetics have a 3-7-fold higher odds ratio of severe disease and death after MERS-CoV
58 infection[11, 14-16]. Mouse models of disease and viral infections have been used for studying
59 coronaviruses and other pathogens[20]. MERS-CoV also demonstrated increased morbidity and

60 mortality in an obese/diabetic mouse model, with high fat diet (HFD) mice presenting with increased
61 lung pathology, viral titer, and a dysregulated immune response to MERS-CoV infection [11, 19, 21].
62 The etiology of type 2 diabetes is closely linked with chronic inflammation induced by excess
63 adipose tissue. Stressed adipocytes and adipose tissue macrophages (ATMs) secrete numerous
64 proinflammatory cytokines that result in chronic low-grade inflammation which alters homeostatic
65 glucose regulation by decreasing cellular responsiveness to insulin[4]. This results in hyperglycemia,
66 hyperinsulinemia, and glucose intolerance characteristic of type 2 diabetes (T2D). The systemic
67 inflammatory responses of obesity and T2D are seen in the microenvironment of the lungs. Polarization
68 of the macrophage response is observed where a Th1 response predominates in OB/OB and DIO
69 mice[22, 23]. It is shown that fewer macrophages are recruited to the lungs which allows for the
70 inflammatory response to recruit other cell types, including neutrophils which we observe in this
71 manuscript[24, 25]. This systemic inflammatory response leads to altered vaccine responses for a variety
72 of vaccines in humans and can be observed in mice. Through several studies, the role of T cells is
73 dominant where vaccinated obese or diabetic mice have reduced T cell activation thus altering the
74 vaccine efficacy[26]. The mechanism underlying these deficiencies are currently unknown.
75 To study the role of obesity and diabetes in SARS-CoV-2, we utilized a mouse model where mice
76 are fed a high fat diet (60% fat from diet) starting at 3 weeks of age compared to a normal diet (ND)
77 (22% fat from diet). By 14 weeks of age, HFD mice are obese, glucose intolerant and have high resting
78 glucose levels; all metrics of having Type 2 diabetes (T2D). Infection of ND and HFD mice with SARS-CoV-
79 2 (MA10 mouse adapted strain) demonstrates lethal disease in HFD only mice by 7 dpi. Equivalent viral
80 lung titers were found in both ND and HFD mice, but increased lung inflammation was observed in HFD
81 (obese/diabetic) mice. Vaccination of ND and HFD mice with the saponin-based Matrix-M adjuvanted
82 spike nanoparticle (NVX-CoV2373)[27, 28] resulted in generation of similar levels of neutralizing
83 antibody. However, when challenged with SARS-CoV-2 (MA10), HFD mice had a delay in clearance with
84 little reduction in lung titer. Evaluation of the inflammatory response in HFD vaccinated/infected mice
85 found an increase in neutrophils in lung infiltrate that correlated with an increased innate inflammatory
86 response. When neutrophils are depleted in HFD mice we observed reduced weight loss, reduced
87 clinical signs of disease and increased survival demonstrating a role for neutrophils in severity of disease
88 in diabetic/obese mice. We conclude this demonstrates a dysregulated immune response in
89 obese/diabetic mice leading to increased morbidity and mortality as well as potentially skewing the
90 quality of protection from vaccination. This supports what is seen in diabetic and obese humans

91 throughout the COVID-19 pandemic and provides a model to identify the molecular and immunological
92 mechanisms underlying the response to SARS-CoV-2 in this population.
93
94 **Results**
95 **High fat diet fed mice have obesity and type 2 diabetes**
96 To study the effects of obesity and diabetes on SARS-CoV-2 infection, we established a model of
97 SARS-CoV-2 infection based on the previously established HFD fed model. At the time of weaning (~3
98 weeks), C57BL/6 mice are placed on a ND (18% kcal from fat, 24% kcal from protein, and 58% kcal from
99 carbohydrates) or a HFD (60% kcal from fat, 18% kcal from protein, and 21% from carbohydrates)
100 (Figure 1A). At 18 weeks of age, 15 weeks on each diet, we analyzed fasting blood glucose (Figure 1B),
101 weight (Figure 1C) and *ACE2* expression (Figure 1D). The HFD mice had increased fasting blood glucose
102 and higher weight, which are all parameters of obesity, insulin resistance and T2D. We examined the
103 expression of *ACE2* to ensure there were no intrinsic differences that could confound results during
104 infection. We did not observe any difference in ACE2 levels in normal vs obese/diabetic mouse cohorts.
105 Once established, 18-week-old ND and HFD mice were then used for pathogenesis and vaccination
106 experiments throughout the study.
107
108 **SARS-CoV-2 infected obese/diabetic mice have increased morbidity and mortality**
109 ND and HFD mice were infected with the SARS-CoV-2 (MA10) strain [29] at $10^3$ and $10^5$ PFU per
110 mouse. Mice were weighed daily for 7 days, with lungs evaluated on 2-, 4- and 7-days post-infection
111 (dpi). ~20% of the ND mice infected with $10^3$ or $10^5$ PFU MA10 died by 7 dpi compared to the HFD mice
112 infected with $10^3$ PFU where ~40% die by day 7 (Figure 2A). Most notably, 100% death was observed in
113 the $10^5$ PFU infected HFD group. The kinetics of lethality varied between groups as well, with 20% of the
114 HFD mice dying by day 3 whereas the ND mice did not die until 5 dpi.
115 Weight loss was followed through 7 dpi in all groups (Figure 2B-E). For the low infection dose,
116 we observed the ND mice starting to lose weight at 2 dpi with a total weight loss of 20% by 7 dpi. The
117 HFD mice lost weight starting 2 dpi, which continued until 4dpi, for a total loss of around 10% and was
118 maintained for the remainder of the experiment. For the high infection dose, the ND mice lost weight
119 starting on 2 dpi and continued through the day 7 endpoint of this experiment with a total weight loss of
120 ~30% (Figure 2C). The HFD mice lost weight starting on 2 dpi and continued until succumbing to the
121 infection on 5 dpi (Figure 2C). As ND mice weigh less than HFD mice, analysis of by grams of weight lost

122 intra group, as compared to total %, can provide additional insight. Here, when we compare the ND and
123 NFD mice, no differences were observed (Figure 2D & E).
124 We next examined viral replication in the lungs of infected mice at 2, 4, and 7 dpi. For all groups,
125 the peak viral replication occurred at 2 dpi with a viral titer ~$10^8$ pfu/g of lung and decreased through
126 day 7 (Figure 2F). At 4 dpi, we observed less viral titer in the $10^5$ PFU group compared to the $10^3$ PFU
127 group (Figure 2F). This was surprising; however, we suspect that the reduced viral titer in the high dose
128 lungs is potentially due to either reduced numbers of infectable cells at this timepoint due to virus
129 induced cell death or a large influx of inflammatory cells, potentially limiting replication but not to
130 substantial levels or quality to protect from death.
131
132 **Obese/diabetic mice have altered host immune responses after infection with SARS-CoV-2**
133 As obesity/diabetes is known to augment the host immune response[30-34], we examined the
134 cytokine and chemokine profile of uninfected, SARS-CoV-2 infected ND and HFD mice to determine if
135 differences in immune response correlated with disease. To perform a longitudinal analysis, we used the
136 samples from mice infected with $1x10^3$ pfu/mouse across 7 dpi. qPCR was performed on lung RNA, and
137 we investigated the changes in expression for a variety of chemokine and cytokine genes in both ND and
138 HFD mice. On days 2 and 4 post-infection, we observed a neutrophil recruitment associated chemokines
139 in HFD compared with ND mice (Figure 2G). Cxcl1, Cxcl10, Csf3 and IL10 are all key neutrophil
140 recruitment factors and are highly upregulated in HFD mice at day 2 of infection. Those levels are
141 reduced at day 4 and then lower at day 7. This correlates with the neutrophil infiltration kinetics seen in
142 the lungs as shown in Figure 4. Interestingly, we observe that HFD mice had a ~5 fold down-regulation of
143 IL1-β, which is a mediator of lung inflammation, fever and fibrosis and is associated with protection in
144 human COVID19 patients (Figure 2G). We hypothesize that neutrophils play an early and critical role in
145 protection from lethal disease in this model and that reduction of neutrophils may protect mice from
146 lethal disease.
147
148 **Obese/diabetic mice have no difference in lung pathology after infection with SARS-CoV-2**
149 At the low infectious dose, both HFD and ND mice show similar lung pathology characterized by
150 a mixed inflammatory infiltrate that peaks at 4 dpi and begins to resolve by 7 dpi. Epithelial cell
151 sloughing in the bronchi is observed starting at 2 dpi with epithelial cells replaced by 7 dpi in most large
152 airways. An observable level of edema is also visible in both HFD and ND lungs across time points (Figure
153 3A).

154 At the high infectious dose, the course of inflammation in the lung is similar but more severe
155 than at the low dose. Mixed inflammatory infiltrates in the alveolar space are observed beginning at 2
156 dpi and increasing through 7 dpi for the surviving ND mice. The infiltrates are predominantly comprised
157 of neutrophils and monocytes, as observed by H&E and quantified by flow cytometry analysis in Figure
158 7. Bronchiolar sloughing is also more pronounced at the high infectious dose, with visible damage still
159 present at 7 dpi. Perivascular cuffing and edema were also observed in the high infectious dose mice
160 (Figure 3A).
161 Lung sections were stained for the presence of nucleocapsid (N) protein using
162 immunohistochemistry to visualize viral antigen localization within the lung sections and to determine if
163 HFD caused broader spread of infection than ND fed mice. Similar to what was observed by viral titer,
164 the amount of N staining is highest at 2 dpi, with the majority of N localizing in the ciliated epithelial
165 cells of the large airways for both the control and HFD mice (Figure 3B). We detect a small amount of N
166 positivity outside the airways, most noticeably at 4 dpi (Figure 3B). Sections from 7 dpi show little to no
167 N staining positivity, correlating with the viral clearance pattern observed by the viral titer (Figure 3B).
168 No differences are observed between ND and HFD mice demonstrating that HFD mice have no change in
169 virus tropism. This data demonstrates that obesity/diabetes increases the mortality of a SARS-CoV-2
170 infection.
171
172 **Vaccinated HFD mice suffer from weight loss and have delayed clearance after SARS-CoV-2 infection**
173 Obesity/diabetes decreases vaccine efficacy towards viral respiratory pathogens [30-36]. In
174 humans receiving SARS-CoV-2 mRNA vaccination, those with obese/diabetic co-morbidity demonstrate
175 the highest rates of severe disease and hospitalization [37-40]. Thus, to mimic the timing of vaccination
176 in the general population, we assessed the efficacy of a clinically licensed adjuvanted protein subunit
177 vaccine (NVX-CoV2373) vaccine in obese/diabetic mice. NVX-CoV2373 is an adjuvanted full-length Spike
178 protein vaccine based on the SARS-CoV-2/Wuhan1 sequence that is highly effective at reducing SARS-
179 CoV-2 infection in young ND mice[28]. At 18 weeks of age, ND and HFD mice were vaccinated with 1 µg
180 of NVX-CoV2373 and then received a second dose 14 days later. On day 28 post-vaccination, blood was
181 collected to evaluate neutralizing antibodies towards SARS-CoV-2 (MA10). On day 32 (~2 weeks after 2$^{nd}$
182 vaccination), mice were challenged with $1x10^5$ pfu/mouse of SARS-CoV-2 (MA10) (Figure 4A). The $1x10^5$
183 pfu is lethal in obese/diabetic mice by 7 dpi, as seen in Figure 2A, so for this experiment the mice were
184 only analyzed through 4dpi. We monitored weight daily and analyzed lungs on 2 and 4 dpi to determine
185 viral lung titer and immune responses (Figure4A). As expected, the unvaccinated mice had no detectable

186 neutralizing antibodies against MA10 (Figure 4B). Vaccinated ND mice had ~ $1x10^4$ neut99, as did the
187 vaccinated HFD mice (Figure 4B), demonstrating no difference between groups. Next, we observed that
188 non-vaccinated mice in both ND or HFD mouse groups had ~ 50% survival rate by day 3, with no further
189 mortality through 4dpi (Figure 4C). Unvaccinated ND mice lost 10% of their starting weight through 4dpi
190 (Figure 4D), which was prevented with vaccination. However, vaccination in HFD mice did not protect
191 from a ~10% starting weight loss by 4dpi.
192 Lungs of infected mice were next analyzed for viral titer at 2 and 4dpi. The unvaccinated ND
193 mice had a viral titer of ~$10^{10}$ pfu/g (Figure 4F) and other than 2 mice with moderate levels in their
194 lungs, cleared the virus by 2dpi. By 4dpi, the unvaccinated ND mice had 2 logs lower virus compared to 2
195 dpi, and the vaccinated ND mice had almost no detectable virus in their lungs (Figure 4F). For the HFD
196 mice, at 2 dpi, there was little difference in lung titer between vaccinated and unvaccinated mice even
197 though these mice had equivalent levels of neutralizing antibody (Figure 4F). At 4dpi, the unvaccinated
198 HFD mice had equivalent lung titers to the ND mice, and the vaccinated HFD mice had no detectable
199 virus in their lungs (Figure 4F). This demonstrates that despite comparable neutralizing titers in
200 vaccinated HFD and ND mice, there is significantly delayed clearance of SARS-CoV-2 in obese/diabetic
201 mice.
202
203 **HFD mice have increased neutrophil infiltration and higher inflammatory chemokine response after**
204 **SARS-CoV-2 infection**
205 Our data demonstrating that HFD mice suffer from increased weight loss and have delayed
206 clearance suggests they have a distinct immune response that alters infection. To assess the innate
207 immune response of HFD mice after challenge with SARS-CoV-2, we performed both flow cytometry
208 based immunophenotyping and quantification of cytokine and chemokine protein levels in the lungs.
209 Our previous analysis RNA levels in the lungs of obese/diabetic mice suggested that neutrophils may be
210 present at much higher concentration in obese/diabetic lungs.
211 As obesity is known to augment the immune system, we established the baseline immune cell
212 population in the lungs of uninfected ND and HFD mice to determine what the initial skew was of
213 inflammatory infiltrates. When we examined the cells of the innate immune system, we observed HFD
214 mice had about 5-fold fewer neutrophils and 3-fold fewer monocyte-derived dendritic cells (moDCs)
215 compared to ND mice (Figure 5A & 5C). For adaptive immune system cells, we observed that HFD mice
216 had around 2-fold higher total T cells, $CD4^+$, and $CD8^+$ T cells (Figure 6 C-E). With established baselines,

217 we could examine how infection and infection plus vaccination change the landscape of the immune
218 cells.
219 As neutrophils are the first cell recruited to the site of infection, we quantified the percentage of
220 neutrophils in the lungs. On day 2 post-infection, unvaccinated HFD mice recruited ~5-fold the
221 neutrophils to the lungs as compared to uninfected HFD mice (Figure 5A). Interestingly, this recruitment
222 was to the level of unvaccinated ND mice, which did not increase neutrophil recruitment compared to
223 uninfected (Figure 5A). On day 4 post-infection, around a 5-fold decrease in neutrophils was observed
224 between the sham HFD and ND mice, which indicated the HFD mice had returned to baseline (Figure
225 6A). To determine if other innate immune system cells were augmented during infection, we next
226 examined the different subsets of DCs. Regardless of vaccine status, ND and HFD had ~20-fold increase
227 in $CD11b^+$ DCs and ~2-fold decrease in $CD103^+$ DCs compared to uninfected. We did not observe changes
228 in the moDCs of ND vaccinated or unvaccinated compared to uninfected ND mice (Figure 6C). However,
229 on day 2 post-infection, sham-vaccinated HFD mice had around a 3-fold increase in moDCs compared to
230 uninfected, which was comparable to ND uninfected mice (Figure 5C). On day 4 post-infection, the
231 unvaccinated ND mice had ~3-fold higher moDCs than vaccinated ND mice. Collectively, this data
232 demonstrates that HFD mice preferentially recruit neutrophils to the site of infection. Their immune
233 system is below the baseline of ND mice and must compensate for this. After examining myeloid lineage
234 cells, we wanted to determine how cells of lymphoid origin responded to infection.
235 NK cells are lymphoid origin but are cells of the innate immune system and could play a role in
236 the differential protection seen. Unvaccinated ND mice had about a significant 6-fold increase of NK cells
237 at day 2 post-infection, with a trend at day 4 post-infection compared to uninfected (Figure 6A).
238 Vaccinated ND mice did not increase their percentage of NK cells compared to unvaccinated, which is
239 not surprising as vaccination should elicit a robust adaptive immune response. Regardless of vaccination
240 status, HFD mice had a 2-fold increase of NK cells on day 2 and 4 post infection (Figure 6A). Suggesting
241 that vaccination was not as efficient in these mice. Next, we wanted to examine the cells of the adaptive
242 immune system.
243 For B cells that produce antibodies, we observed that HFD vaccinated mice had ~2-fold higher B
244 cells in their lungs at day 4 post-infection than HFD unvaccinated mice (Figure 6B). Finally, we wanted to
245 examine the T cell response between these mouse groups. When we compared uninfected ND and HFD
246 mice, we observed ~2-fold higher total T cells, $CD4^+$ and $CD^+8$ T cells (Figure 6C-E). We hypothesized that
247 HFD mice had a lower percentage of innate immune cells which allows for the percentage of T cells to
248 contribute more to the overall $CD45^+$ cell population. On day 2 post-infection sham vaccinated ND had

249 ~2-fold higher T cells, $CD4^+$ and $CD8^+$ T cells compared to sham HFD mice (Figure 6C-E), and around 2-
250 fold lower $CD8^+$ T cell compared to ND vaccinated mice (Figure 6E). Vaccinated ND mice had ~2-fold
251 $CD4^+$ T cells compared to HFD vaccinated mice (Figure 6D). On day 2 post-infection unvaccinated HFD
252 mice had ~2-fold less total T cells and $CD4^+$ T cells when compared to HFD and ND vaccinated mice
253 respectively (Figure 6C&D). This data suggests that HFD mice have a lower percentage of T cells
254 compared to ND mice and have a poorer $CD4^+$ T cell response to a challenge after vaccination.
255
256 **HFD mice have altered antigen specific T cell activation**
257 We performed *ex vivo* stimulation of T cells with SARS-CoV-2 spike peptide pool from the lungs
258 of vaccinated and unvaccinated ND and HFD mice. For unvaccinated ND and HFD mice, we observed
259 negligible amounts of cytokine production from $CD4^+$ or $CD8^+$ T cells after stimulation (Figure 6 F&G). It
260 was determined that vaccinated mice production of IFN-γ and TNF-α after peptide stimulation,
261 indicating a T cell response skewed towards a $Th_1$ response (Figure 6 F&G). For HFD vaccinated mice,
262 IFN-γ and TNF-α were secreted from $CD4^+$ and $CD8^+$ T cells, but only $CD8^+$ T cells significantly increased
263 compared to unvaccinated (Figure 6 F&G). However, ND vaccinated mice produced IFN-γ and TNF-α
264 from $CD4^+$ and $CD8^+$ T cells and produced more from $CD4^+$ T cells compared to HFD mice (Figure 7 F&G).
265 Taken together, vaccination induces a $Th_1$ response in ND and HFD mice, but vaccination does not
266 induce a robust response in HFD mice compared to ND mice which collaborates with could be due to
267 lower percentage of $CD4^+$ T cell in HFD mice (Figure 6D).
268
269 **HFD Mice have higher levels of cytokine and chemokines in the lungs after challenge**
270 To further characterize the immune responses in ND and HFD mice, we next performed
271 a multiplexing cytokine assay to examine the concentration of soluble immune mediators in the lungs of
272 vaccinated ND and HFD SARS-CoV-2 infected mice. When we compared the ND and HFD mice at 2 dpi,
273 we observed higher levels of CCL2, CCL5, CCL7, CXCL10, and IL-6, and at 4dpi, CCL2, CCL5, CXCL12,
274 CXCL1, GM-CSF, and TNF-α in HFD mice compared to ND mice (Figure 7). These chemokines are all
275 produced from or attract neutrophils and are concordant with the increased neutrophil infiltration we
276 observe in flow cytometry analysis of infected mice. As we observed this infiltration of neutrophils in
277 HFD mice compared to ND mice, we wanted to determine if neutrophils played a role in the increased
278 mortality of HFD mice.
279 To address the role neutrophils play in the increased mortality of HFD mice, we depleted
280 neutrophils with an anti-Ly6G antibody (clone, 1A8) in the context of a lethal ($1x10^5$ pfu/mouse) SARS-

281 CoV-2 mouse model. A day before infection, mice were intra-peritoneally injected with either anti-Ly6G
282 or control (IgG2a isotype) antibody, and administration continued every other day throughout the
283 infection. We examined mortality as our first parameter to determine the effect neutrophils have on
284 increased mortality in HFD mice. ND mice with neutrophils depleted compared to isotype control
285 showed no differences in survivability (Figure 8A). However, HFD mice lacking neutrophils demonstrated
286 increased survivability compared to HFD isotype and anti-Ly6G ND mice (Figure 8A). After determining
287 the effect on mortality, we wanted to examine weight loss. HFD mice given the isotype antibody lost
288 around 10 percent body weight, which was similarly observed in the previous study (Figure 8B & 2C). As
289 previously observed, ND mice lost around 30 percent of their body weight (Figure 8B & 2C). Neutrophil
290 depleted ND mice lost around 20 percent of body weight before death (Figure 8B & 2C). Surprisingly,
291 neutrophil depleted HFD mice lost around 10 percent body weight, but they survived to the
292 experiment's conclusion, which was not previously observed (Figure 8B & 2C). This data suggests that
293 neutrophil recruitment has a direct role the increased mortality of SARS-CoV-2 infection.
294
295 **Discussion**
296 SARS-CoV-2 infection is more severe in obese and diabetic individuals[5-7, 21]. This has been
297 observed in epidemiological data across many countries and economic levels[8]. Increased disease in
298 diabetic and obese individuals is seen following several viral infections, including Influenza virus,
299 Hepatitis B, Hepatitis C, and another highly pathogenic coronavirus, MERS-CoV[19, 41, 42]. We have
300 previously demonstrated that in a mouse model of MERS-CoV, there is increased inflammation and a
301 dysregulated immune response[18]. In this work, we utilized an obese and diabetic mouse model for the
302 study of SARS-CoV-2 pathogenesis to determine whether we could observe increased disease as well as
303 assess the effect of obesity and diabetes on SARS-CoV-2 vaccine responses.
304 We find that there are significant differences in the obese and diabetic (HFD) mice compared to
305 normal mice after SARS-CoV-2 infection. First, the HFD mice have increased mortality after SARS-CoV-2
306 infection compared to ND mice. There are no observed differences in lung pathology or virus titer to
307 explain the reason for the mortality other than the increased neutrophil infiltration we observed in the
308 lungs of mice, which may have an overreaching effect on other aspects of host response not accounted
309 for in this work.
310 Upon vaccination of the ND and HFD mice, we identify severe effects of obesity and diabetes on
311 the vaccine mediated protection in mice. While neutralizing antibody levels are similar between ND and
312 HFD mice vaccinated with NVX-2373 and lethality is protected in both the ND and HFD vaccinated mice,

313 even with their advanced age to the initial testing, there is no protection from weight loss in the
314 vaccinated HFD mice compared to ND mice. When virus levels in the lung were analyzed, we observe a
315 significant delay in clearance of virus at 2 dpi with the HFD mice showing no reduction in virus titer of
316 vaccinated mice while the ND mice reduce virus titer by 4 logs in lungs at the same timepoint. Analysis
317 of the inflammatory response in the mice also shows differences with the key difference being higher
318 levels of neutrophils in the lungs of sham and vaccinated HFD mice compared to ND mice. This was
319 corroborated by assaying for chemokines and cytokines in these lungs. We find that neutrophil
320 produced chemokines and cytokines are significantly upregulated in the HFD mice, potentially
321 associated with the reduction in clearance of virus from HFD vaccinated mice. Analysis of adipose tissue
322 in humans also displays increased inflammation which correlates with what we observe in mice[43, 44].
323
324 We interpret these results to demonstrate that the HFD mouse model reflects what is seen in
325 humans with obesity and diabetes throughout the COVID-19 pandemic. This comorbid population has
326 significantly more hospitalizations, irrespective of vaccine status. This model also allows us to begin to
327 differentiate the mechanism behind this lack of protection from SARS-CoV-2. The receptor for SARS-
328 CoV-2 is ACE2 and in humans there is a modest increase in ACE2 levels in some reports suggesting that
329 increased disease could be due to increased entry and thus infection with SARS-CoV-2[45]. In mice, we
330 do not see an increase in ACE2 levels in lungs in the diabetic and obese model used here. While this
331 could be a reason for increased disease in diabetic humans, we do not believe this is the reason for
332 increased disease that we see in mice. With equivalent neutralizing antibody levels but less clearance in
333 lungs, we hypothesize that this is due to changes in quality of the antibodies produced. Potentially the
334 antigens that the antibodies recognize, or the subtypes of the antibodies are changed in the
335 obese/diabetic mice compared to normal mice. There are reports of altered T cell activation in humans
336 with obesity in response to COVID19 vaccination suggesting that T cells may be involved in the altered
337 inflammatory response as well[46]. We also observe the strong association of a hyperactive neutrophil
338 response in the lungs. This could either be due to increased neutrophil recruitment or once there the
339 neutrophils are not responding correctly. We have shown that depleting neutrophils in diabetic/obese
340 mice protects them from lethal disease suggesting neutrophil activity in the lungs is pathologic in this
341 model.
342 We hypothesize that the dysregulated immune response leads to increased morbidity and
343 mortality as well as skewing the ability of antibodies produced by vaccination to clear viral infection. It is
344 yet to be determined whether it is the metabolic disease associated with obesity that is driving this

345 response or the hyperglycemia of type 2 diabetes however alterations to therapeutic efficacy from
346 vaccination to anti-viral drugs can be affected by either type of metabolic change and will be studied
347 further in the future.
348
349 **Methods**
350 **Cells and Virus Strain:**
351 Virus and cells were processed as described previously [47]. Briefly, Vero E6 cells (ATCC# CRL 1586) were
352 cultured in DMEM (Quality Biological), supplemented with 10% (v/v) fetal bovine serum (Gibco), 1%
353 (v/v) penicillin/streptomycin (Gemini Bio-products) and 1% (v/v) L-glutamine (2 mM final concentration,
354 Gibco) (Vero media). Cells were maintained at 37°C and 5% $CO_2$. SARS-CoV-2 (MA10) was provided by
355 Dr. Ralph Baric (UNC). Stocks were prepared by infection of VeroE6 cells for two days when CPE was
356 starting to be visible [48]. Media were collected and clarified by centrifugation before being aliquoted
357 for storage at −80°C. The stock titer was determined by plaque assay using Vero E6 cells as described
358 previously [49]. All work with infectious virus was performed in a Biosafety Level 3 laboratory and
359 approved by our Institutional Biosafety Committee.
360
361 **Animal Ethics Statement:**
362 The University of Maryland School of Medicine is accredited by the Association for Assessment and
363 Accreditation of Laboratory Animal Care (AAALAC International). All animal procedures were in
364 accordance with NRC Guide for the Care and Use of Laboratory Animals, the Animal Welfare Act, and
365 the CDC/NIH Biosafety in Microbiological and Biomedical Laboratories. Mouse studies were approved
366 by The University of Maryland School of Medicine IACUC. Studies were conducted in accordance with
367 the National Institutes of Health Guide for Care and Use of Laboratory Animals (NIH publication 8023,
368 Revised 1978). All mouse infections are carried out in an animal BSL-3 facility in accordance with
369 approved practices.
370
371 **Husbandry of diet induced obesity mice**
372 18-weeks-old male C57BL/6 diet included obesity (DIO) and C57BL/6 control mice were purchased from
373 Jackson Laboratory. After arrival, mice were kept on a diet of normal chow (22% kcal from fat; Teklad,
374 2019S) or a diet consisting of high fat chow (60% kcal from fat; Teklad, TD.06414) and maintained on
375 their respective diets throughout the course of the experiments. To evaluate the diabetic status of the
376 mice their fasting blood glucose and starting weight were evaluated before infection. Animals were

377 fasted with water only for six hours prior glucose testing to obtain fasting blood glucose
378 measurements. Sub-mandibular blood was used to obtain blood glucose measurements on a Contour
379 One blood glucose meter strip (Ascensia, Parsippany, NJ).
380
381 **Mouse Infections:**
382 18-weeks-old male C57BL/6 diet included obesity (DIO) and C57BL/6 control mice were purchased from
383 Jackson Laboratory. On day 0, mice were anesthetized by intraperitoneal injection 50 µL of a mix of
384 xylazine (0.38 mg/mouse) and ketamine (1.3 mg/mouse) diluted in phosphate-buffered saline (PBS).
385 While anesthetized, mice were intranasally inoculated with either 50 µL sterile PBS, 1 x $10^3$ PFU or
386 1x$10^5$ PFU of SARS-CoV-2 MA10. Mice are monitored daily for weight loss and signs of morbidity. On
387 days 2, 4, and 7, animals were euthanized, and lung tissue was collected for further analysis.
388
389 **Mouse Challenge Study:**
390 18-weeks-old male C57BL/6 diet included obesity (DIO) and C57BL/6 control mice were purchased from
391 Jackson Laboratory and immunized by intramuscular (IM) injection with two doses spaced 14 days apart
392 (day 0 and 14) of 1 µg rS-WU1, with 5 µg saponin-based Matrix-M™ adjuvant (Novavax, AB, Uppsala, SE)
393 as a prime/boost. A placebo group was injected with vaccine formulation buffer as a negative control.
394 Serum was collected for analysis on days 0 and 28. Vaccinated and control animals were intranasally
395 challenged with SARS-CoV-2 on study day 32. On days 2 and 4 post-challenge, animals were euthanized,
396 and lung tissue was collected for further analysis.
397
398 **Histology & Immunohistochemistry:**
399 Lung sections were fixed in 4% paraformaldehyde (PFA) in phosphate-buffered saline (PBS) for a
400 minimum of 48 h, after which they were sent to the Histology Core at the University of Maryland,
401 Baltimore, for paraffin embedding and sectioning. Five-micrometer sections were prepared and used
402 for hematoxylin and eosin (H&E) staining by the Histology Core Services.
403 For SARS-CoV-2 nucleocapsid immunohistochemistry staining, five-micrometer sections were cut from
404 paraffin-embedded blocks and placed onto positively charged slides. The sections were immunostained
405 using the Dako EnVision FLEX + detection system (DAKO, Carpinteria, CA). The Dako PT link was used for
406 deparaffinization and heat-induced epitope retrieval using Dako Target Retrieval Solution, High pH, for
407 20 minutes. Endogenous peroxidase activity was blocked with DAKO Peroxidase-Blocking Reagent for 5
408 min before incubation with rabbit polyclonal SARS Nucleocapsid Protein Antibody [NB100-56576]

409 (Novus Biologicals, Centennial, CO), 1:400 for 20 minutes at room temperature, followed by DAKO Anti-
410 rabbit HRP Detection Reagent for 20 minutes. Finally, the sections were incubated for 10 min with DAKO
411 diaminobenzene (DAB) before they were counterstained with Dako FLEX hematoxylin, rinsed, and
412 mounted in Cytoseal XYL (Thermo Scientific, Waltham, MA). Sections were imaged at 10x magnification,
413 and figures were put together using Adobe Photoshop and Illustrator software (Adobe, San Jose, CA).
414
415 **Plaque Assay:**
416 VeroE6/TMPRSS2 cells were cultured in DMEM (Quality Biological), supplemented with 10% (v/v) heat-
417 inactivated fetal bovine serum (Sigma), 1% (v/v) penicillin/streptomycin (Gemini Bio-products), and 1%
418 (v/v) L-glutamine (2 mM final concentration, Gibco) (Vero Media). Cells were maintained at 37°C (5%
419 $CO_2$). SARS-CoV-2 lung titers were quantified by homogenizing mouse lungs in 1ml phosphate-buffered
420 saline (PBS; Quality Biological Inc.) using 1.0mm glass beads (Sigma Aldrich) and a Beadruptor (Omni
421 International Inc). VeroE6 cells are plated in 12 well plates with $1.5x10^5$ cells per well. SARS-CoV-2
422 virus titer in plaque forming units was determined by plaque assay. In the plaque assay, 25 µl of the
423 lung homogenate is added to 225 µl of DMEM and diluted 10-fold across a 6-point dilution curve with
424 200ul of diluent added to each well. After 1 hour, a 2 ml agar overlay containing DMEM is added to
425 each well. Plates are incubated for three days at 37°C (5% $CO_2$) before plaques are counted.
426
427 **SARS-CoV-2 Neutralization Titer Determination:**
428 SARS-CoV-2 neutralizing antibody titers were determined as described previously [50]. Briefly, serum
429 samples were heat-inactivated to remove complement and allowed to equilibrate to room temperature
430 before processing. Samples were diluted in duplicate for a 12-point, 1:2 dilution series with an initial
431 dilution of 1:40 dilution (1:80 following virus addition). Dilution plates were then transported into the
432 BSL-3 laboratory, and equal volume SARS-CoV-2 inoculum was added to each plate. A non-treated, virus-
433 only control and a mock infection control were included on every plate. The sample/virus mixture was
434 then incubated at 37°C (5.0% $CO_2$) for 1 hour before transferring to 96-well titer plates with confluent
435 VeroE6 cells. Titer plates were incubated at 37°C (5.0% $CO_2$) for 72 hours, followed by CPE
436 determination for each well in the plate. The first sample dilution to show CPE was reported as the
437 minimum sample dilution required to neutralize >99% of the concentration of SARS-CoV-2 tested
438 (neut99).
439
440 **Gene Expression:**

441 Mouse lung tissue was homogenized in 1 mL of TRIzol (Ambion) using 1.4-mm glass beads (Omni
442 International, Inc.) and a beadruptor (Omni International, Inc.) RNA was extracted using the DIRECT-zol
443 Mini RNA Extraction kit (Zymo Research) per the manufacturer's instructions. RNA was transcribed into
444 cDNA using $RT^2$ First Strand Kit (Qiagen). Gene expression was performed using Real-time PCR for $RT^2$
445 Profile PCR Array Mouse Cytokine and Chemokines using $RT^2$ SYBR® Green Mastermixes (Qiagen). Using
446 the $RT^2$ qPCR Array Data Analysis spreadsheet, gene expression was calculated using the ΔΔCt method
447 with housekeeping genes as the control, and fold-change calculated relative to control mice infected
448 lungs. Fold-regulation, which represents fold-change in a biologically meaningful way, was calculated
449 using fold change. A fold-change value greater than one indicates an up-regulation, and the fold-
450 regulation is equal to the fold change. A fold-change value less than one indicates a down-regulation,
451 and the fold-regulation is negative inverse of the fold-change.
452
453 **Cytokine and Chemokine Quantification:**
454 For the quantification of secreted cytokine and chemokines induced by SARS-CoV-2 infection, mice lung
455 tissue was homogenized in 1 mL of PBS (Quality Biologicals, Inc.) using 1.4-mm glass beads (Omni
456 International, Inc.) and a beadruptor (Omni International, Inc.). Bio-Plex Pro Mouse Chemokine Panel
457 31-plex (BIORAD) was used to quantify cytokines and chemokines in lung homogenate according to the
458 manufacturer's protocol with the addition of a fixation step after the final wash. Samples underwent a
459 24-hour fixation (4 % formaldehyde, Sigma-Aldrich) at 4°C. After fixation, the plate was washed three
460 times in wash buffer, microparticles were resuspended in 100 µL wash buffer, and analyzed on a
461 Luminex MagPix and xPONENT Software version 4.3. Based on the standard curve, concentrations
462 (pg/mL) of each analyte were calculated for all samples.
463
464 **Flow Cytometry:**
465 Single cells were isolated from lungs using the Lung Dissociation Kit, mouse and gentleMACS Dissociator
466 (Miltenyi Biotec). Lungs were placed in C tubes (Miltenyi Biotec) containing 2.2 mL Buffer S, 15 µL of
467 Enzyme A, and 100 µL of Enzyme D. Lungs were run on m_lung_01 and allowed to digest for 30 minutes
468 at 37°C followed by running m_lung_02. Cell suspensions were filtered on a 70-µm filter (BD), and cells
469 were pelleted by centrifugation. Red blood cells were lysed in ammonium-chloride-potassium lysis
470 buffer (Quality Biological, Inc.) and subsequently washed with PBS containing 3% FBS. Approximately,
471 $1x10^6$ cells were plated and washed twice with PBS containing. Cells were stained for viability using the
472 Live/Dead Fixable NIR Dead Cell Stain Kit (Molecular Probes). Cells were washed with PBS containing 3%

473 FBS. Cells were stained with antibody cocktails made in BD Horizon Brilliant Stain Buffer (BD). The
474 antibodies used were as follows: CD45 Alexa Fluor 700 (BioLegend, clone 30-F11), CD11b Brilliant Violet
475 650 (BioLegend, clone M1/70), Ly6G Brilliant Violet 785 (BioLegend , clone 1A8), Ly6C Brilliant Violet
476 510 (BioLegend, clone HK1.4), CD3 BUV 563 (BD, clone 145-2C11), CD4 FITC (BioLegend, clone
477 GK1.5), CD8a APC (BioLegend clone 53-6.7), CD19 PE (BioLegend clone 6D5), and NK1.1 Pacific Blue
478 (BioLegend, clone PK136), CD65 Brilliant Violet 605 (BioLegend, clone X54-5/7.1), CD103 BUV 661 (BD,
479 clone 2e7), Siglec-H BUV 563 (BD, clone 440c), and Siglec-F Brilliant Violet 711 (BD, clone E50-2440).
480 Stained cells were washed twice and fixed for 1 hour in FluoroFix (BioLegend). For Intracellular Cytokine
481 Staining, lung leukocytes $2x10^6$ cells/well from vaccinated and sham mice were cultured at 37°C for 5
482 hours in the presence of SARS-CoV-2 spike peptide pool (1µg/mL) kindly provided by Alessandro Sette
483 LA Jolla Institute, Brefeldin A and Monensin (BioLegend). The peptide pool consisted of overlapping 15-
484 mers by 10 spanning entire protein. The treated cells were incubated with LIVE/DEAD Fixable NIR Dead
485 Cell stain (Invitrogen) for 20 min at room temperature. Cells were then labeled for cell surface markers
486 at 4°C for 15 minutes in the dark followed by fixation and permeabilization for 20 min at 4°C (BD
487 CytoFix/CytoPerm) then labeled with intracellular antibody cocktail. The antibodies used were as
488 follows: IFN-γ BV421 (BioLegend, clone: XMG1.2), TNF-α BV650 (BioLegend, clone:MP6-XT22), IL-4
489 BV605 (BioLegend, clone: 11B11), and IL-17a BV711 (BioLegend, clone: TC11-18H10.1). Fixed cells were
490 washed once in PBS containing 3% FBS and resuspended in PBS containing 3% FBS. Samples were
491 acquired (approximately 50,000 events) using the Aurora-UV spectral flow cytometer (Cytek), and data
492 were analyzed using FCS Express analysis software (DeNova Software, Pasadena, CA).

493 **Neutrophil Depletion:**

494 18-weeks-old male C57BL/6 diet included obesity (DIO) and C57BL/6 control mice were purchased from
495 Jackson Laboratory and neutrophils were depleted with 500 µg of anti-Ly6G (clone 1A8) or isotype
496 antibody (IgG2a isotype) (Bio-X-Cell, Lebanon, NH), via i.p. injection 1 day prior to infection with SARS-
497 CoV-2 and every two days afterwards. Mice were infected with either 50 µL sterile PBS or $1x10^5$ PFU of
498 SARS-CoV-2 MA10. Mice are monitored daily for weight loss and signs of morbidity. On day 7, animals
499 were euthanized, and lung tissue was collected for further analysis.
500

501 **Statistical Analysis:**

502 Statistical analyses were performed with GraphPad Prism 9.2 software (GraphPad Software, San Diego,
503 CA). Data were analyzed using unpaired t-test, Log-rank (Mantel-Cox) test, one-way or two-way ANOVA

504 followed by Tukey, Sidak, or Dunnett multiple comparison post-hoc test as indicated. All statistical
505 analysis were two-sided and a $p < 0.05$ was consisted as statistically significant.
506
507 **Competing/Conflict of Interest**
508 M.B.F. is on the scientific advisory board of Aikido Pharma and has collaborative research agreements
509 with Novavax, AstraZeneca, Regeneron, and Irazu Bio. These do not have any effect on the planning or
510 interpretations of the work presented in this manuscript. N.P. and G.S are employees of Novavax.
511
512 **Financial Support**
513 This work is partially funded by NIH R01 AI148166, NIH HHSN272201400007C, NIH
514 HHSN272201400008C/ 0258-0689-4609 to M.B.F. RJ is funded by T32AI007524. N.P. and G.S are
515 employees of and funded by Novavax.
516

517 **Figure Legends**
518 **Figure 1: A high fat diet induces obesity and diabetes in C57BL/6J mice.**
519 **A**. Schematic overview illustrating diet schedule and infection for control and obese/diabetic mice.
520 Briefly, at weaning (3 weeks), mice were placed on a normal diet (ND) or high fat diet (HFD). At 18 weeks
521 of age, these mice were infected with either $1x10^3$ or $1x10^5$ pfu of SARS-CoV-2 Mouse Adaptive 10,
522 monitored daily for weight changes, and a subset was euthanized at day 2, 4, and 7 to analyze lung viral
523 titer and host immune response. The **B.** fasted blood glucose concentration *n=13* mice/group, **C.** The
524 starting weight of ND and HFD mice *n=45* mice/group, and **D.** *ACE2* expression of ND and HFD mice *n=5*
525 mice/group prior to infection. * $p <0.5$ and **** $p < 0.0001$ as determined by an unpaired two-sided t-
526 test. The data are presented as mean ± SD.
527
528 **Figure 2: Enhanced mortality in obesity/ diabetes mice after SARS-CoV-2 infection.**
529 The survival (A), percent weight loss for low dose (B), high dose (C), grams lost for low dose (D), and high
530 dose (E) challenge. Viral lung titers were assessed for control and obese/ diabetic mice throughout a
531 SARS-CoV-2 MA10 infection (F). For **A.** * $p < 0.05$ as determined by a Log-rank (Mantel-Cox) test for
532 survival analysis between ND and HFD for low and high infection dose with the data presented as mean
533 ± SD with *n=10* mice/group. In G, lung cytokine, chemokine, and growth factors were assessed at 2, 4,
534 and 7 dpi for the $1x10^3$ infectious dose using a mouse cytokine/chemokine array. The fold change was

535 calculated compared to ND infected mice (n=3). For **B-D** the data are presented as mean ± SD with *n*=3-5
536 mice/group.
537
538 **Figure 3: Similar lung histology and viral clearance in control and obese/ diabetic mice.**
539 Control and obese/diabetic mice were infected intranasally with either $1x10^3$ or $1x10^5$ pfu/ mouse.
540 Lungs were collected on 2, 4, and 7 dpi and fixed in 10% neutral buffered formalin for greater than 24
541 hours. Tissue was embedded in paraffin. **A.** 5 µm sections were cut and stained with hematoxylin and
542 eosin, and **B.** immunostained with anti-SARS Nucleocapsid Protein antibody. Images are shown at
543 original magnification x10 and are representative of *n* = 3-5 mice/group.
544
545 **Figure 4: Viral clearance is delayed in obese/ diabetic vaccinated mice.**
546 **A.** Schematic overview illustrating vaccination and challenge for ND and HFD mice. Briefly, at 18 weeks
547 of age, mice were vaccinated as well as 14 days later. On day 28 post-vaccination, mice were bled to
548 determine **B.** serum neutralizing antibodies prior to infection, *n* = 12-15 mice/group. On day 32, these
549 mice were challenged with $1x10^5$ pfu of SARS-CoV-2 MA 10, monitored daily for weight changes, and a
550 subset was euthanized on day 2 and 4 to analyze lung viral titer and host immune response. The **C.**
551 mortality, weight loss of **D.** ND, **E.** HFD, and **F.** viral titer of sham and vaccinated mice after SARS-2 MA10
552 challenge. *n*= 5-10 mice/group. For **D**, * $p < 0.5$ and *** $p < 0.001$ as determined by a mixed-effect
553 analysis followed by a Sidak test for multiple comparisons. For **F.** p *** $< 0.001$ and p **** $< 0.0001$,
554 data were log-transformed and analyzed by mixed-effect analysis followed by Sidik for multiple
555 comparisons. The data are pooled from 2 independent experiments and presented as mean ± SD.
556
557 **Figure 5: Increased neutrophil recruitment in the lungs of HFD mice after SARS-CoV-2 challenge.**
558 After SARS-2 MA10 challenge, lungs were harvested, cells isolated, and stained for surface markers for
559 **A.** neutrophils, **B.** $CD11b^+$ DCs, **C.** monocyte-derived DCs, **D.**$CD103^+$ cDCs, **E.** plasmacytoid DCs at day 2
560 and 4 post-challenge. * $p < 0.05$ and ** $p < 0.01$ as data were analyzed by mixed-effect analysis followed
561 by Tukey for multiple comparisons *n*=3-5 mice/group.
562
563 **Figure 6: T cell dysregulation in the lungs of HFD mice after SARS-CoV-2 challenge.**
564 After SARS-2 MA10 challenge, lungs were harvested, cells isolated, and stained for surface markers for
565 **A.** Natural Killer cells, **B.** B cells**, C.** Total T cells, **D.** T helper cells, **E.** Cytotoxic T cells at day 2 and 4 post-
566 challenge *n*=3-5 mice/group. * $p < 0.05$ as data were analyzed by mixed-effect analysis followed by

567 Tukey for multiple comparisons *n*=3-5 mice/group **F.** $CD4^+$ SARS-CoV-2-specific T cells and **G.** $CD8^+$ SARS-
568 CoV-2 specific T cells from naïve and vaccinated ND and HFD mice after *ex-vivo* stimulation *n*=6
569 mice/group * p <0.5 as determined by an unpaired two-sided t-test. The data are presented as mean ±
570 SD.
571
572 **Figure 7: Increased neutrophil recruitment and cytokine production in HFD vaccinated mice after**
573 **challenge.** On day 2,4,7 dpi, lungs were harvested and used in a Bio-plex pro mouse chemokine panel.
574 The pg/mL was generated from a standard curve. * $p < 0.05$ and ** $p < 0.01$ as analyzed by mixed-effect
575 analysis followed by Sidak for multiple comparisons *n*=3-5 mice/group.
576
577 **Figure 8: Increased HFD survival with neutrophil depletion after challenge.** The **A.** survival and percent
578 weight loss for **B.** isotype antibody control or **C.** anti-Ly6G antibody ND and HFD mice. * $p < 0.05$ as
579 analyzed by Gehan-Breslow-Wilcoxon test for survival *n*=5 mice/group.

580

581 **References**

582

583


584 1. CDC. *National Diabetes Statistics Report*. Available from:
585 https://www.cdc.gov/diabetes/data/statistics-report/index.html.
586 2. Esser, N., et al., *Inflammation as a link between obesity, metabolic syndrome and type 2*
587 *diabetes.* Diabetes Res Clin Pract, 2014. **105**(2): p. 141-50.
588 3. Ritchie, S.A. and J.M. Connell, *The link between abdominal obesity, metabolic syndrome and*
589 *cardiovascular disease.* Nutr Metab Cardiovasc Dis, 2007. **17**(4): p. 319-26.
590 4. Grundy, S.M., *Obesity, metabolic syndrome, and cardiovascular disease.* J Clin Endocrinol Metab,
591 2004. **89**(6): p. 2595-600.
592 5. Kompaniyets, L., et al., *Body Mass Index and Risk for COVID-19-Related Hospitalization, Intensive*
593 *Care Unit Admission, Invasive Mechanical Ventilation, and Death - United States, March-*
594 *December 2020.* MMWR Morb Mortal Wkly Rep, 2021. **70**(10): p. 355-361.
595 6. Apicella, M., et al., *COVID-19 in people with diabetes: understanding the reasons for worse*
596 *outcomes.* Lancet Diabetes Endocrinol, 2020. **8**(9): p. 782-792.
597 7. Rawshani, A., et al., *Severe COVID-19 in people with type 1 and type 2 diabetes in Sweden: A*
598 *nationwide retrospective cohort study.* Lancet Reg Health Eur, 2021. **4**: p. 100105.
599 8. Ozonoff, A., et al., *Phenotypes of disease severity in a cohort of hospitalized COVID-19 patients:*
600 *Results from the IMPACC study.* EBioMedicine, 2022. **83**: p. 104208.
601 9. Heubner, L., et al., *Extreme obesity is a strong predictor for in-hospital mortality and the*
602 *prevalence of long-COVID in severe COVID-19 patients with acute respiratory distress syndrome.*
603 Sci Rep, 2022. **12**(1): p. 18418.

604 10. Rosero, P.A., et al., *Risk Factors for COVID-19: A Systematic Mapping Study.* Stud Health Technol
605 Inform, 2022. **299**: p. 63-74.
606 11. Badawi, A. and S.G. Ryoo, *Prevalence of Diabetes in the 2009 Influenza A (H1N1) and the Middle*
607 *East Respiratory Syndrome Coronavirus: A Systematic Review and Meta-Analysis.* J Public Health
608 Res, 2016. **5**(3): p. 733.
609 12. Rathnasinghe, R., et al., *The N501Y mutation in SARS-CoV-2 spike leads to morbidity in obese and*
610 *aged mice and is neutralized by convalescent and post-vaccination human sera.* medRxiv, 2021.
611 13. Johnson, R.M., et al., *Diet Induced Obesity and Diabetes Enhance Mortality and Reduces Vaccine*
612 *Efficacy for SARS-CoV-2.* bioRxiv, 2022.
613 14. Assiri, A., et al., *Epidemiological, demographic, and clinical characteristics of 47 cases of Middle*
614 *East respiratory syndrome coronavirus disease from Saudi Arabia: a descriptive study.* Lancet
615 Infect Dis, 2013. **13**(9): p. 752-61.
616 15. Cha, R.H., et al., *Renal Complications and Their Prognosis in Korean Patients with Middle East*
617 *Respiratory Syndrome-Coronavirus from the Central MERS-CoV Designated Hospital.* J Korean
618 Med Sci, 2015. **30**(12): p. 1807-14.
619 16. Choi, W.S., et al., *Clinical Presentation and Outcomes of Middle East Respiratory Syndrome in the*
620 *Republic of Korea.* Infect Chemother, 2016. **48**(2): p. 118-26.
621 17. Gao, Y.D., et al., *Risk factors for severe and critically ill COVID-19 patients: A review.* Allergy,
622 2021. **76**(2): p. 428-455.
623 18. Kulcsar, K.A., et al., *Comorbid diabetes results in immune dysregulation and enhanced disease*
624 *severity following MERS-CoV infection.* JCI Insight, 2019. **4**(20).
625 19. Yang, Y.M., et al., *Impact of Comorbidity on Fatality Rate of Patients with Middle East*
626 *Respiratory Syndrome.* Sci Rep, 2017. **7**(1): p. 11307.
627 20. Rydell-Tormanen, K. and J.R. Johnson, *The Applicability of Mouse Models to the Study of Human*
628 *Disease.* Methods Mol Biol, 2019. **1940**: p. 3-22.
629 21. Alanazi, K.H., et al., *Diabetes Mellitus, Hypertension, and Death among 32 Patients with MERS-*
630 *CoV Infection, Saudi Arabia.* Emerg Infect Dis, 2020. **26**(1): p. 166-168.
631 22. Lee, F.Y., et al., *Phenotypic abnormalities in macrophages from leptin-deficient, obese mice.* Am J
632 Physiol, 1999. **276**(2): p. C386-94.
633 23. Manicone, A.M., et al., *Diet-induced obesity alters myeloid cell populations in naive and injured*
634 *lung.* Respir Res, 2016. **17**: p. 24.
635 24. O'Brien, K.B., et al., *Impaired wound healing predisposes obese mice to severe influenza virus*
636 *infection.* J Infect Dis, 2012. **205**(2): p. 252-61.
637 25. Milner, J.J., et al., *Diet-induced obese mice exhibit altered heterologous immunity during a*
638 *secondary 2009 pandemic H1N1 infection.* J Immunol, 2013. **191**(5): p. 2474-85.
639 26. Bandaru, P., H. Rajkumar, and G. Nappanveettil, *Altered or Impaired Immune Response to*
640 *Hepatitis B Vaccine in WNIN/GR-Ob Rat: An Obese Rat Model with Impaired Glucose Tolerance.*
641 ISRN Endocrinol, 2011. **2011**: p. 980105.
642 27. Guebre-Xabier, M., et al., *NVX-CoV2373 vaccine protects cynomolgus macaque upper and lower*
643 *airways against SARS-CoV-2 challenge.* Vaccine, 2020. **38**(50): p. 7892-7896.
644 28. Tian, J.H., et al., *SARS-CoV-2 spike glycoprotein vaccine candidate NVX-CoV2373 immunogenicity*
645 *in baboons and protection in mice.* Nat Commun, 2021. **12**(1): p. 372.
646 29. Leist, S.R., et al., *A Mouse-Adapted SARS-CoV-2 Induces Acute Lung Injury and Mortality in*
647 *Standard Laboratory Mice.* Cell, 2020. **183**(4): p. 1070-1085 e12.
648 30. Paich, H.A., et al., *Overweight and obese adult humans have a defective cellular immune*
649 *response to pandemic H1N1 influenza A virus.* Obesity (Silver Spring), 2013. **21**(11): p. 2377-86.
650 31. Kim, Y.H., et al., *Diet-induced obesity dramatically reduces the efficacy of a 2009 pandemic H1N1*
651 *vaccine in a mouse model.* J Infect Dis, 2012. **205**(2): p. 244-51.

652 32. Costanzo, A.E., et al., *Obesity impairs gammadelta T cell homeostasis and antiviral function in*
653 *humans.* PLoS One, 2015. **10**(3): p. e0120918.
654 33. Fisher-Hoch, S.P., C.E. Mathews, and J.B. McCormick, *Obesity, diabetes and pneumonia: the*
655 *menacing interface of non-communicable and infectious diseases.* Trop Med Int Health, 2013.
656 **18**(12): p. 1510-9.
657 34. Hagau, N., et al., *Clinical aspects and cytokine response in severe H1N1 influenza A virus*
658 *infection.* Crit Care, 2010. **14**(6): p. R203.
659 35. Painter, S.D., I.G. Ovsyannikova, and G.A. Poland, *The weight of obesity on the human immune*
660 *response to vaccination.* Vaccine, 2015. **33**(36): p. 4422-9.
661 36. Tagliabue, C., et al., *Obesity: impact of infections and response to vaccines.* Eur J Clin Microbiol
662 Infect Dis, 2016. **35**(3): p. 325-31.
663 37. Caimi, B., et al., *Sero-survey on long-term care facility residents reveals increased risk of sub-*
664 *optimal antibody response to BNT162b2: implications for breakthrough prevention.* BMC Geriatr,
665 2022. **22**(1): p. 191.
666 38. Soetedjo, N.N.M., et al., *Antibody response following SARS-CoV-2 vaccination among patients*
667 *with type 2 diabetes mellitus: A systematic review.* Diabetes Metab Syndr, 2022. **16**(2): p.
668 102406.
669 39. Anand, S., et al., *SARS-CoV-2 Vaccine Antibody Response and Breakthrough Infection in Patients*
670 *Receiving Dialysis.* Ann Intern Med, 2022. **175**(3): p. 371-378.
671 40. Mitsunaga, T., et al., *The evaluation of factors affecting antibody response after administration*
672 *of the BNT162b2 vaccine: a prospective study in Japan.* PeerJ, 2021. **9**: p. e12316.
673 41. Almond, M.H., et al., *Obesity and susceptibility to severe outcomes following respiratory viral*
674 *infection.* Thorax, 2013. **68**(7): p. 684-6.
675 42. Honce, R. and S. Schultz-Cherry, *Impact of Obesity on Influenza A Virus Pathogenesis, Immune*
676 *Response, and Evolution.* Front Immunol, 2019. **10**: p. 1071.
677 43. Stefan, N., *SARS-CoV-2 fires up inflammation in adipose tissue.* Nat Rev Endocrinol, 2023. **19**(1):
678 p. 8-9.
679 44. El-Sayed Moustafa, J.S., et al., *ACE2 expression in adipose tissue is associated with cardio-*
680 *metabolic risk factors and cell type composition-implications for COVID-19.* Int J Obes (Lond),
681 2022. **46**(8): p. 1478-1486.
682 45. Wijnant, S.R.A., et al., *Expression of ACE2, the SARS-CoV-2 Receptor, in Lung Tissue of Patients*
683 *With Type 2 Diabetes.* Diabetes, 2020. **69**(12): p. 2691-2699.
684 46. Kelly, N.E.W., et al., *Antigen specific T cells in people with obesity at five months following*
685 *ChAdOx1 COVID-19 vaccination.* Int J Obes (Lond), 2023. **47**(1): p. 83-86.
686 47. Weston, S., et al., *Broad Anti-coronavirus Activity of Food and Drug Administration-Approved*
687 *Drugs against SARS-CoV-2 In Vitro and SARS-CoV In Vivo.* J Virol, 2020. **94**(21).
688 48. Matsuyama, S., et al., *Enhanced isolation of SARS-CoV-2 by TMPRSS2-expressing cells.* Proc Natl
689 Acad Sci U S A, 2020. **117**(13): p. 7001-7003.
690 49. Coleman, C.M. and M.B. Frieman, *Growth and quantification of MERS-CoV infection.* Current
691 Protocols in Microbiology, 2015. **37**(15): p. 2-15.
692 50. Keech, C., et al., *Phase 1-2 Trial of a SARS-CoV-2 Recombinant Spike Protein Nanoparticle*
693 *Vaccine.* N Engl J Med, 2020. **383**(24): p. 2320-2332.
694

# Figure 1

## A)

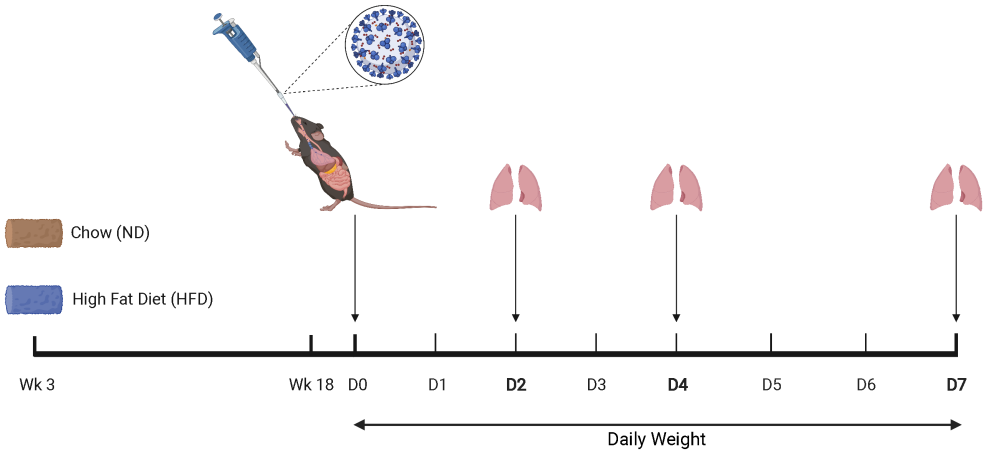


## B) Fasting Blood Glucose

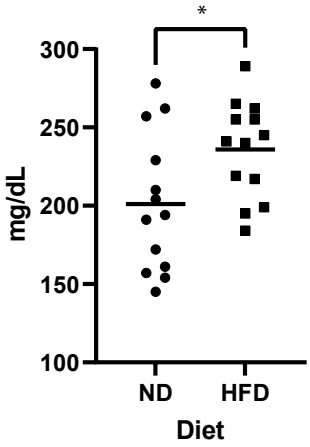


## C) Starting Weight

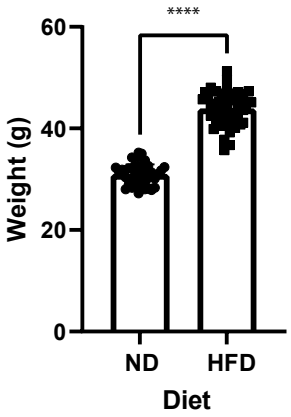


## D) *ACE2*

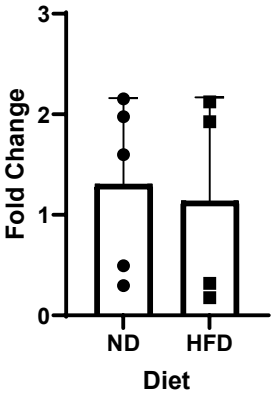

# Figure 2

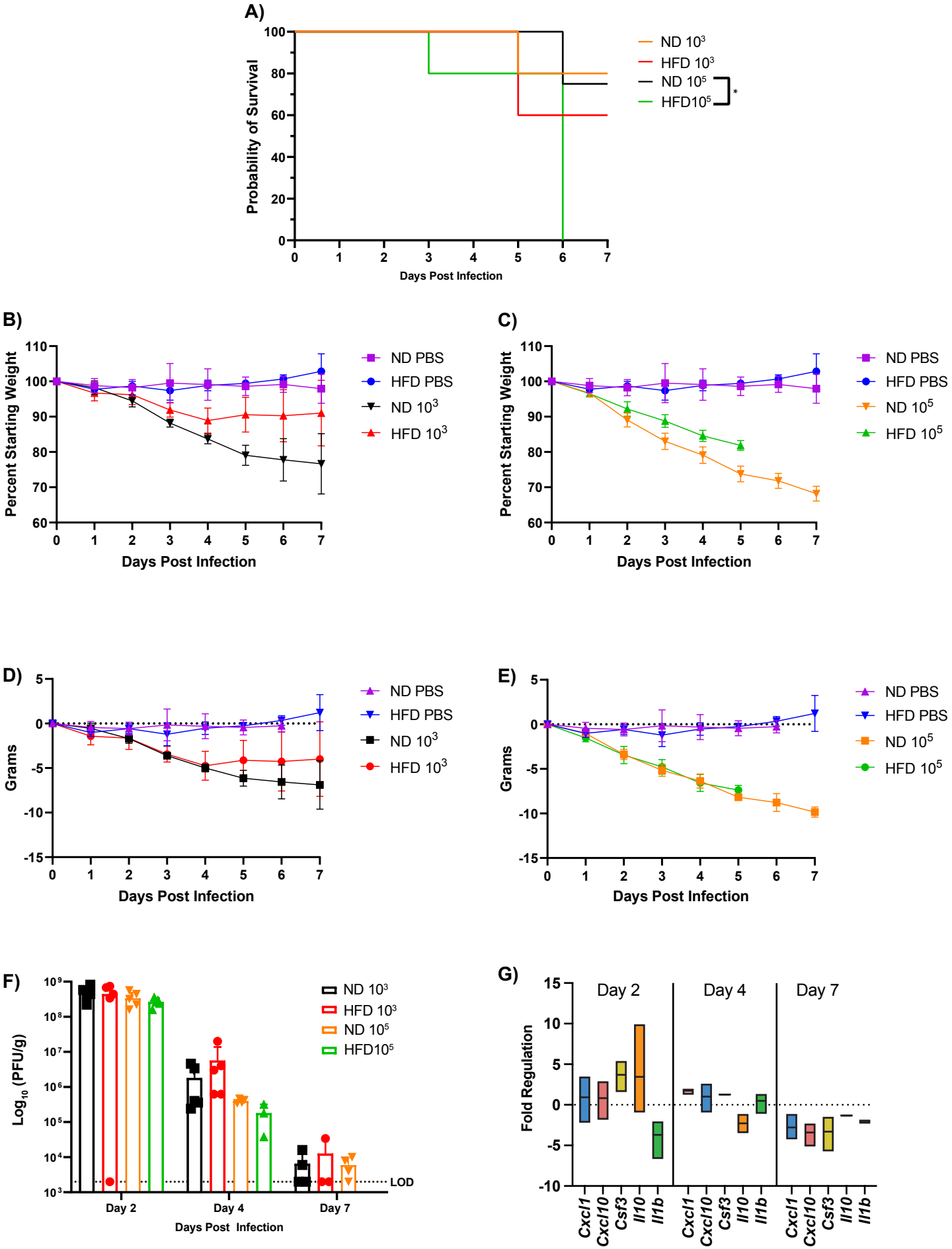
A)
Probability of Survival
Days Post Infection
ND 10³
HFD 10³
ND 10⁵
HFD10⁵
*
B)
Percent Starting Weight
Days Post Infection
ND PBS
HFD PBS
ND 10³
HFD 10³
C)
Percent Starting Weight
Days Post Infection
ND PBS
HFD PBS
ND 10⁵
HFD 10⁵
D)
Grams
Days Post Infection
ND PBS
HFD PBS
ND 10³
HFD 10³
E)
Grams
Days Post Infection
ND PBS
HFD PBS
ND 10⁵
HFD 10⁵
F)
Log10 (PFU/g)
Day 2
Day 4
Day 7
Days Post Infection
LOD
ND 10³
HFD 10³
ND 10⁵
HFD10⁵
G)
Fold Regulation
Day 2
Day 4
Day 7
Cxcl1
Cxcl10
Csf3
Il10
Il1b

# Figure 3

A

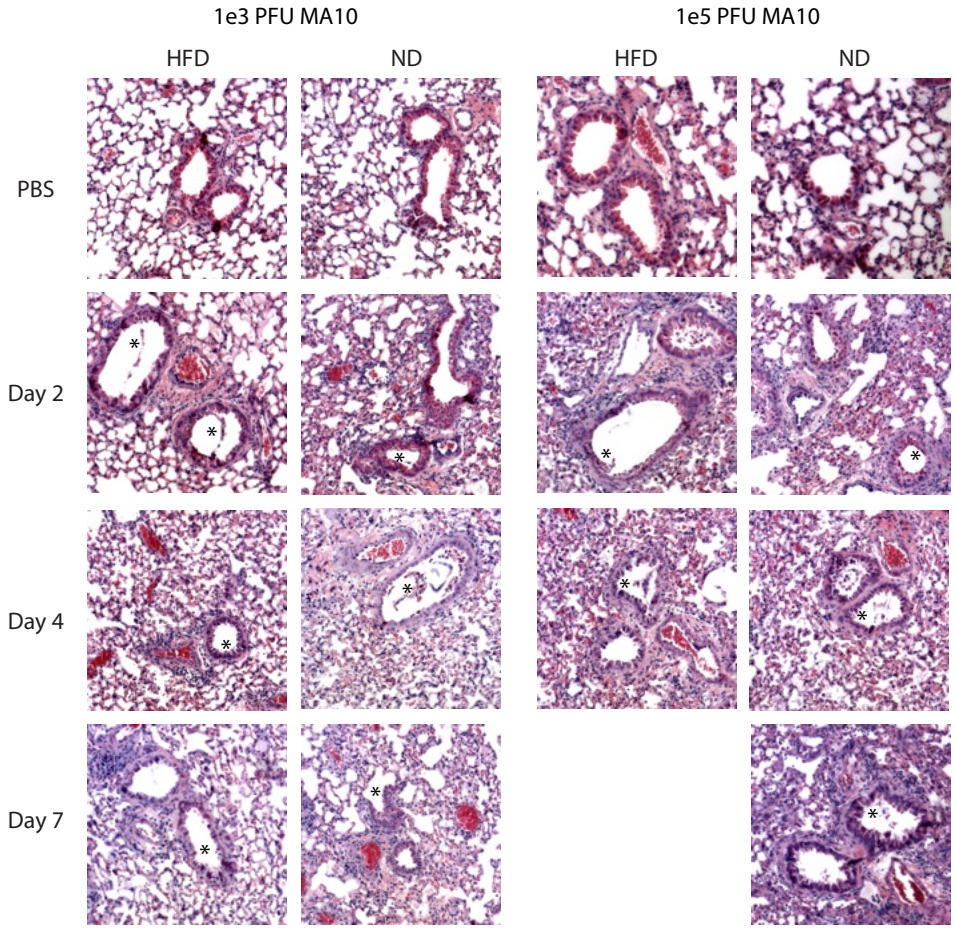
1e3 PFU MA10
1e5 PFU MA10
HFD
ND
HFD
ND
PBS
Day 2
Day 4
Day 7

B

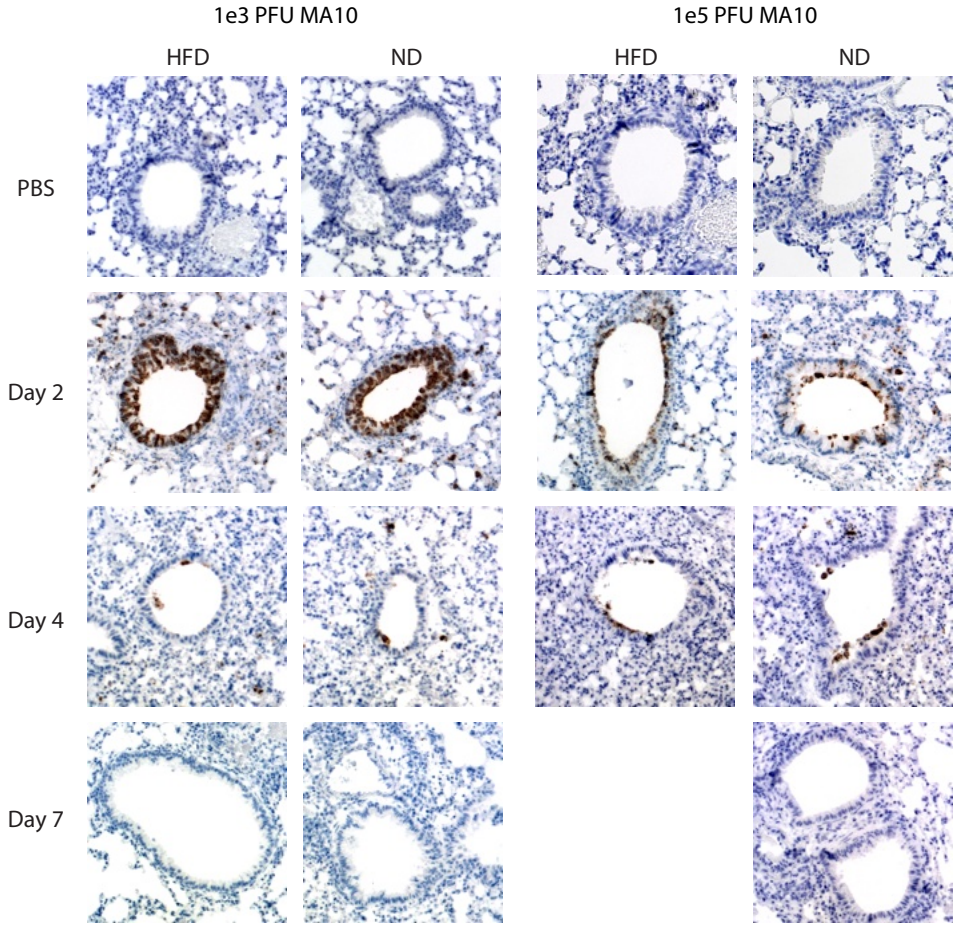
1e3 PFU MA10
1e5 PFU MA10
HFD
ND
HFD
ND
PBS
Day 2
Day 4
Day 7

# Figure 4

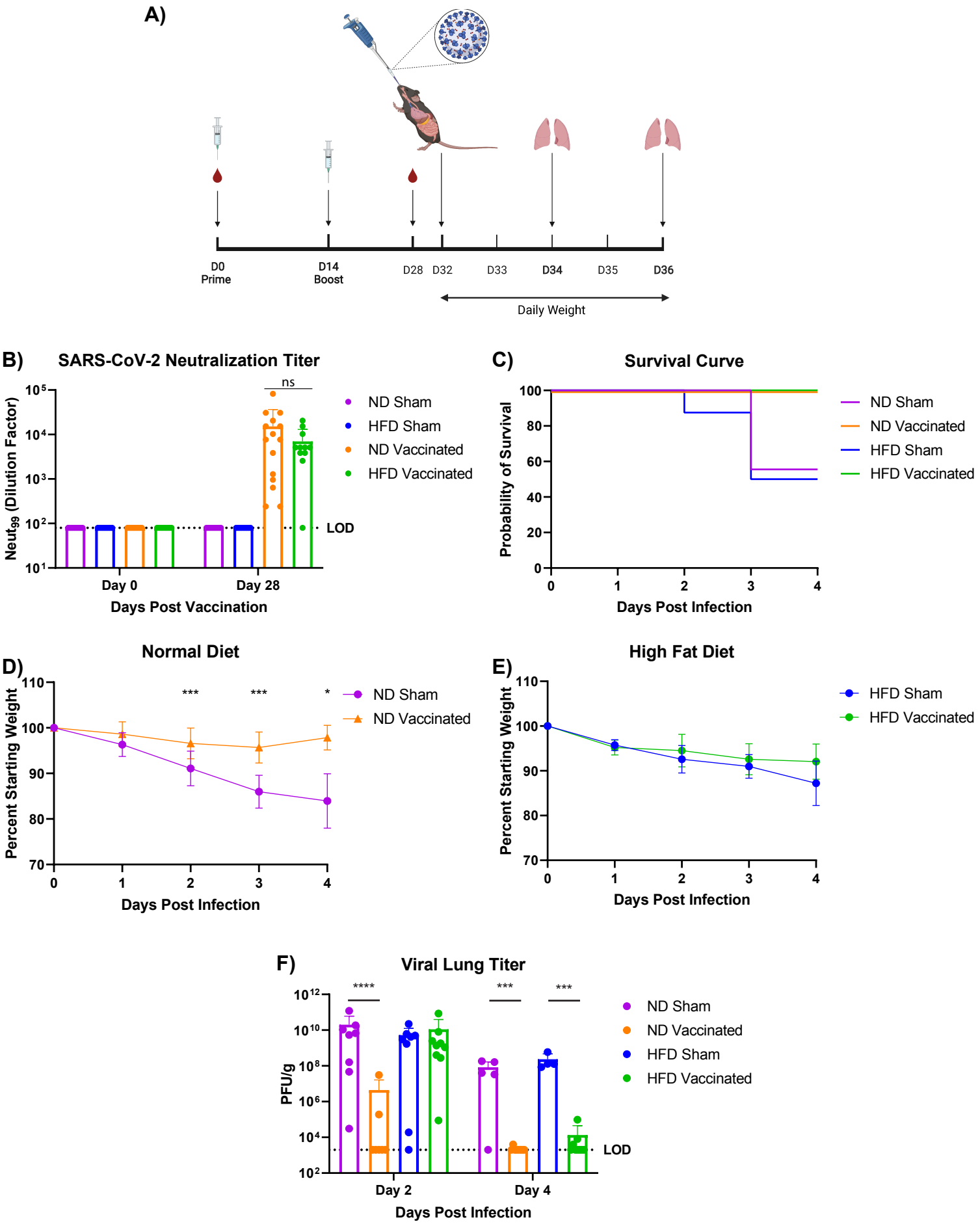
A)
D0
Prime
D14
Boost
D28
D32
D33
D34
D35
D36
Daily Weight
B)
SARS-CoV-2 Neutralization Titer
ns
Neut99 (Dilution Factor)
LOD
Day 0
Day 28
Days Post Vaccination
ND Sham
HFD Sham
ND Vaccinated
HFD Vaccinated
C)
Survival Curve
Probability of Survival
Days Post Infection
ND Sham
ND Vaccinated
HFD Sham
HFD Vaccinated
D)
Normal Diet
Percent Starting Weight
Days Post Infection
ND Sham
ND Vaccinated
E)
High Fat Diet
Percent Starting Weight
Days Post Infection
HFD Sham
HFD Vaccinated
F)
Viral Lung Titer
PFU/g
LOD
Day 2
Day 4
Days Post Infection
ND Sham
ND Vaccinated
HFD Sham
HFD Vaccinated

# Figure 5

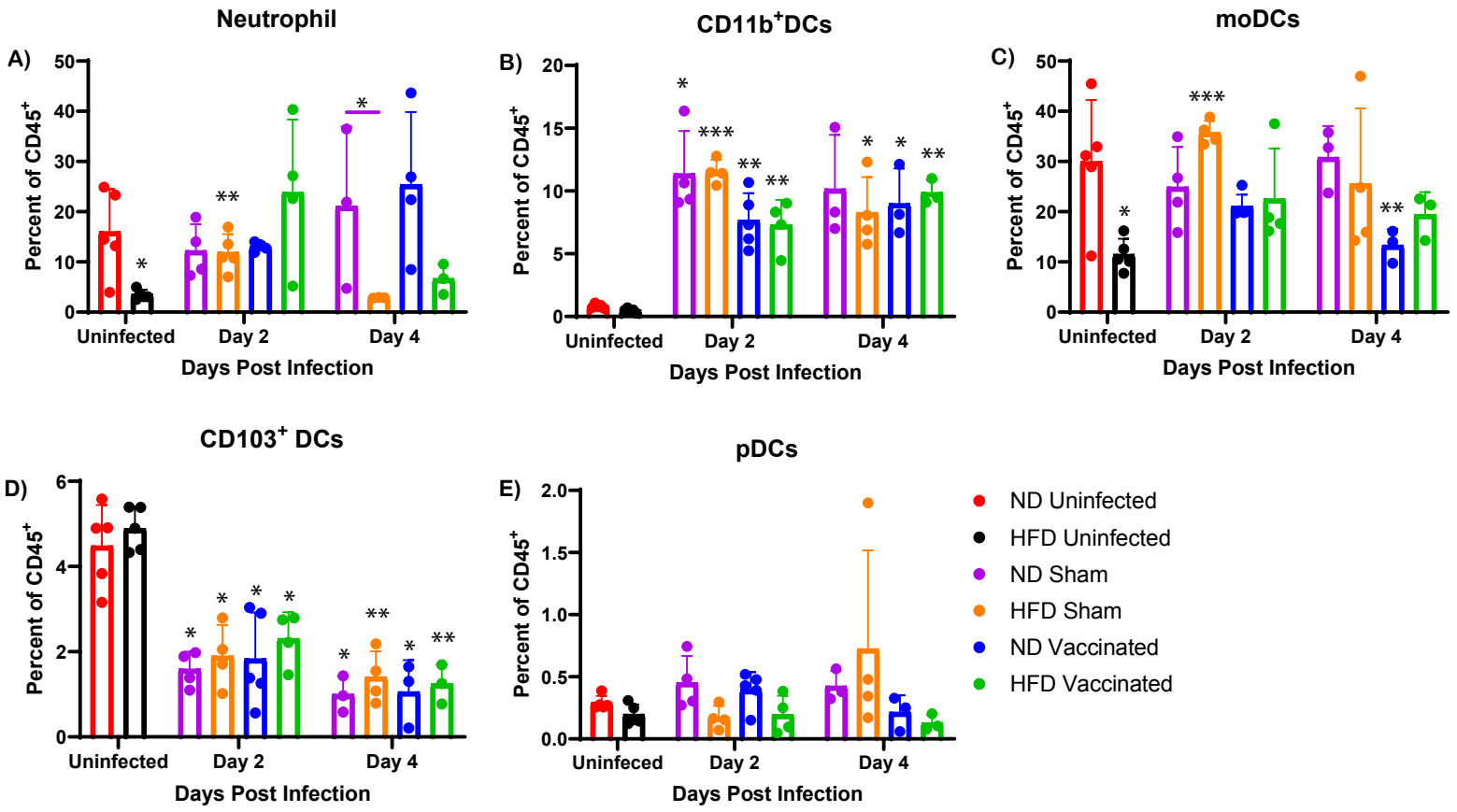
A)
Neutrophil
Percent of CD45+
Uninfected
Day 2
Day 4
Days Post Infection
B)
CD11b+DCs
Percent of CD45+
Uninfected
Day 2
Day 4
Days Post Infection
C)
moDCs
Percent of CD45+
Uninfected
Day 2
Day 4
Days Post Infection
D)
CD103+ DCs
Percent of CD45+
Uninfected
Day 2
Day 4
Days Post Infection
E)
pDCs
Percent of CD45+
Uninfeced
Day 2
Day 4
Days Post Infection
ND Uninfected
HFD Uninfected
ND Sham
HFD Sham
ND Vaccinated
HFD Vaccinated

# Figure 6

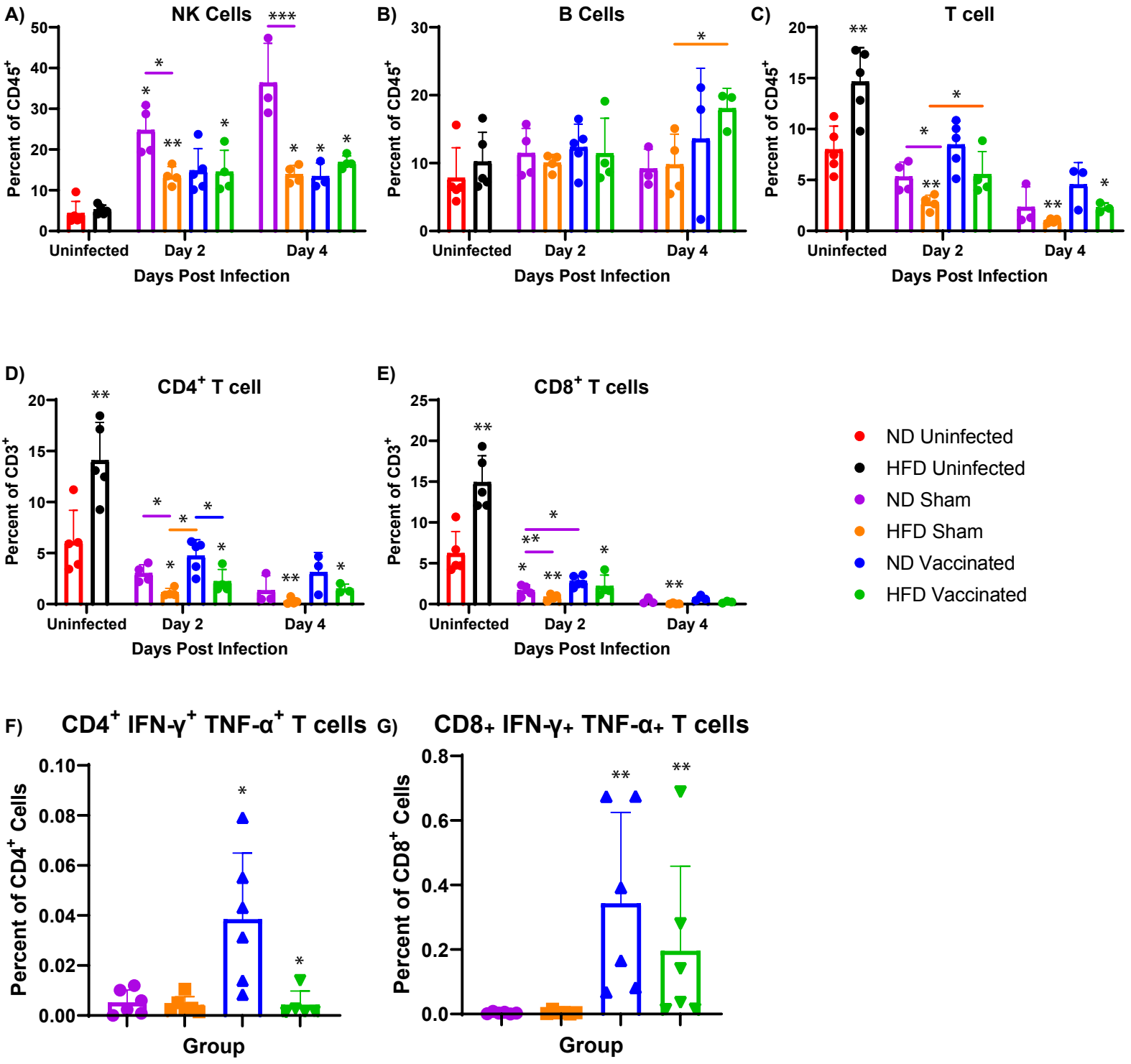
A)
NK Cells
Percent of CD45+
Days Post Infection
Uninfected
Day 2
Day 4
B)
B Cells
C)
T cell
D)
CD4+ T cell
Percent of CD3+
E)
CD8+ T cells
ND Uninfected
HFD Uninfected
ND Sham
HFD Sham
ND Vaccinated
HFD Vaccinated
F)
CD4+ IFN-γ+ TNF-α+ T cells
Percent of CD4+ Cells
Group
G)
CD8+ IFN-γ+ TNF-α+ T cells
Percent of CD8+ Cells

# Figure 7

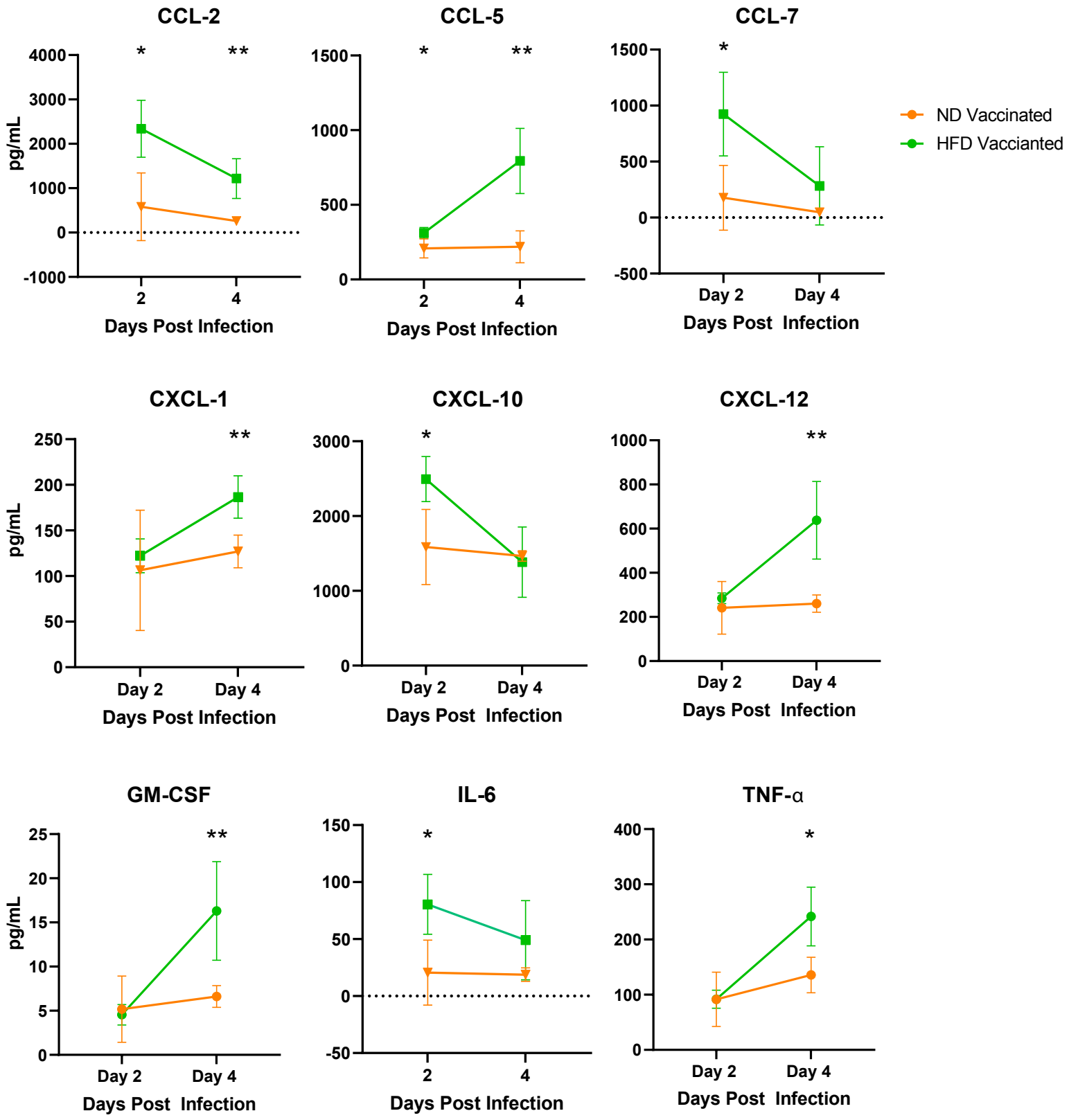
CCL-2
CCL-5
CCL-7
CXCL-1
CXCL-10
CXCL-12
GM-CSF
IL-6
TNF-α
pg/mL
Days Post Infection
Day 2
Day 4
ND Vaccinated
HFD Vaccianted

# Figure 8

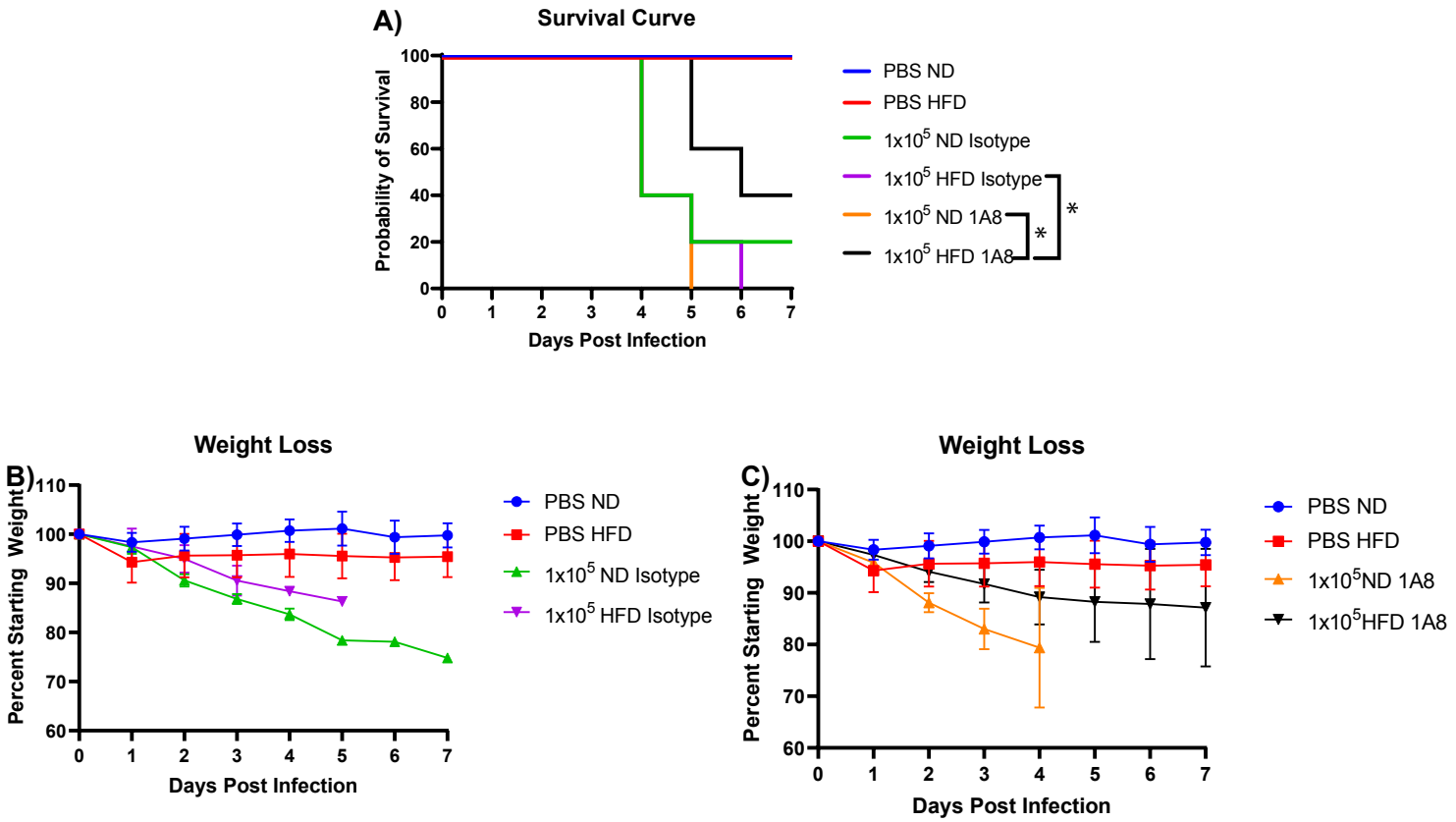
A)
Survival Curve
Probability of Survival
Days Post Infection
PBS ND
PBS HFD
1x10^5 ND Isotype
1x10^5 HFD Isotype
1x10^5 ND 1A8
1x10^5 HFD 1A8
*
*
B)
Weight Loss
Percent Starting Weight
Days Post Infection
PBS ND
PBS HFD
1x10^5 ND Isotype
1x10^5 HFD Isotype
C)
Weight Loss
Percent Starting Weight
Days Post Infection
PBS ND
PBS HFD
1x10^5ND 1A8
1x10^5HFD 1A8